



Cite this: *RSC Adv.*, 2025, 15, 7139

Study on preparation and performance of cement-stabilized macadam containing ground sludge gasification slag (GSGS)

Xiaoyan Zhang,^a Xiaoqi Wang,^a ^a Zhiyong Li,^b Kele Wang,^c Juntao Ma^{*a} and Shunbo Zhao^{*a}

Traditional cement-based road materials face problems of high energy consumption and carbon emissions, and the use of activated solid waste as a substitute for cementitious materials has been applied in road engineering. Sludge gasification slag (SGS), a product obtained from the pyrolysis and gasification of sludge, is a typical silicon–aluminum-rich solid waste that exhibits good compatibility with alkaline activation systems due to its potential activity. This study focuses on the component reconstruction mechanism of SGS in alkali-activated materials, employing cement (P) and carbide slag (CS) for synergistic modification, exploring the mechanism for enhancing the cementitious properties of sludge gasification slag under multi-component mixing conditions, and verifying its feasibility for use in cement-stabilized macadam. The results show that GSGS and GCS have a synergistic activation effect in the cement hydration system, promoting the formation of C–(A)–S–H gel and AFt. When both are incorporated in a mass ratio of 6 : 4 and account for 70% of the composite system, the compressive strength is increased by 53.19% compared to alone. When the composite material is used in cement-stabilized macadam with a 40% replacement ratio of cement, there is no significant decrease in strength, verifying the feasibility of using cement-composite sludge gasification slag in cement-stabilized macadam.

Received 19th January 2025
Accepted 17th February 2025

DOI: 10.1039/d5ra00462d

rsc.li/rsc-advances

1 Introduction

With the acceleration of urbanization and industrialization, sludge production has increased sharply, posing significant challenges to the ecological environment and urgently requiring efficient resource utilization strategies.¹ Although traditional biological wastewater treatment technology can effectively reduce the harmful substances in sludge, high chemical consumption, and large-scale applications are significantly limited.^{2–4} Sludge pyrolysis gasification technology, as a low-energy and low-carbon emission alternative, can convert high-moisture sludge into sludge gasification slag (SGS), achieving a reduction of over 90% in volume, thereby greatly promoting the feasibility of sludge resource utilization.^{5,6}

After high-temperature treatment, SGS becomes a porous granular material with a certain strength. Numerous researchers have explored its potential as an aggregate in building materials. Li *et al.*⁷ utilized SGS as a substitute aggregate to prepare mortar, and Ma *et al.*⁸ employed the full

component of SGS to produce concrete filling, demonstrating the potential of SGS as an aggregate. However, it has relatively low strength, particle size and strength distribution of materials exhibit significant variability. When used as an aggregate substitute, it can easily become a weak point in concrete. Therefore, there is an urgent need to search for a method for the comprehensive resource utilization of its full components.

Although extensive research has been conducted on the application of sludge in composite cementitious materials, including performance impacts and process optimization,^{9–11} these studies primarily focus on single-component sludge, with insufficient exploration into the synergistic utilization of SGS and other industrial wastes (such as carbide slag and fly ash). Furthermore, after high-temperature treatment, SGS exhibits reduced structural order, decreased heavy metal leaching, and demonstrates cementitious activity, sharing similar characteristics with coal gasification slag.¹² Guo *et al.*¹³ and Daggubati *et al.*¹² have further confirmed the feasibility of using gasification slag as a performance enhancer and clinker raw material in the cement industry, indicating that the optimization of gasification slag application technology can enhance resource utilization efficiency.¹⁴

The cement-stabilized macadam (CSM), commonly used in road construction, traditionally employs cement as a binder. However, its high carbon emissions conflict with the goals of green development.^{15–17} Consequently, using low-carbon and

^aInternational Joint Research Lab for Eco-building Materials and Engineering of Henan, North China University of Water Resources and Electric Power, Zhengzhou 450045, China. E-mail: majuntao@ncwu.edu.cn

^bZhengzhou Sewage Purification Co., Ltd, Zhengzhou 450045, China

^cXuchang Innovation Center of Low-Carbon Eco-Building Materials Technology, Zhongyuan Institute of Science and Technology, Zhengzhou 450042, China



low-cost supplementary cementitious materials (SCMs) to replace cement has become a research focus. Li *et al.*¹⁴ and Yue *et al.*¹⁸ have demonstrated the potential of various solid waste materials such as SCM in enhancing the durability, mechanical properties, and environmental safety of CSM. It provides theoretical support for the application of SGS.

Based on that, the study aims to conduct composite modification of sludge gasification slag (SGS) using cement and carbide slag (CS), particularly exploring its application in cement-stabilized macadam. The innovation of this research lies in enhancing the performance of SGS through composite modification and validating its feasibility as a cement substitute, thereby providing a new perspective for the resourceful utilization of sludge gasification slag. Specifically, this study will analyze the strength development patterns of composite cementitious materials with different proportions, utilize X-ray diffraction (XRD), Fourier transform infrared spectroscopy (FTIR), and scanning electron microscopy (SEM) techniques to reveal the mineral composition and micromorphological characteristics of their hydration products, and ultimately prepare cement-stabilized macadam (PSC-CSM) and test their mechanical properties to verify the practical application potential of composite-modified SGS as a cementitious material. This research not only addresses the urgent need for energy conservation and emission reduction but also opens a new pathway for the resource utilization of sludge gasification slag.

2. Materials and methods

Fig. 1 illustrates the detailed testing process and main equipment. First, the materials are ground into ground sludge gasification slag (GSGS) and ground carbide slag (GCS) using a ball mill to enhance their reactive properties. Subsequently, they are used to partially replace cement in composite cementitious materials, which are then applied to cement-stabilized macadam. It evaluates the hydration mechanism in composite

cementitious materials and the performance of cement-stabilized macadam by macro and micro tests.

2.1 Raw materials

The sludge gasification slag used in this study was from the Zhengzhou New District Sewage Treatment Plant; carbide slag was obtained from Haohua Yuhang Chemical Co., Ltd. The cement (P) used was P.O 42.5 ordinary Portland cement from the Henan Tianrui Cement Factory. Both were ground in a ball mill for 30 min to obtain ground sludge gasification slag (GSGS) and ground carbide slag (GCS).

Table 1 summarizes the chemical compositions of GSGS, GCS, and cement. The mineral phase composition of GSGS and GCS is shown in Fig. 2. Quartz and feldspar are the dominant phases in GSGS, whereas $\text{Ca}(\text{OH})_2$ and CaCO_3 are predominant in GCS. Table 2 provides the physical performance indicators of the cement, and Table 3 details the performance characteristics of the aggregates used in cement-stabilized macadam preparation.

2.2 Composite cementitious materials

2.2.1 Mix proportions. Two factors were controlled in the proportions of composite cementitious materials as variable. The first factor was the mass ratio of GSGS to GCS, tested in three levels: 4 : 6, 5 : 5, and 6 : 4. The second factor was the cement dosage, evaluated as 20%, 30%, and 40%. The mix proportions of the composite cementitious materials are presented in Table 4.

2.2.2 Mechanical properties. The paste samples were prepared and cast into molds of dimensions 40 mm × 40 mm × 40 mm, using a water-to-binder ratio of 0.4. The surfaces were covered with plastic film to prevent moisture loss. After 24 hours, samples were demoted and placed in a standard curing room at 20 °C and 95% relative humidity for curing 3 d and 28 d. The compressive strengths of the samples were tested using a DY-208J flexural and compressive testing machine.

2.2.3 Micro-characteristics. Regarding the hydration mechanism of composite cementitious materials, microstructure analysis was conducted on cement paste and the P30-S6C4, P30-S10C0, and P30-S0C10 samples. The samples were treated with alcohol and dried at 45 °C for XRD and FTIR analysis. SEM analysis was performed on 1 cm³ cubes extracted from the center of the samples.

2.3 CSM

2.3.1 Mix proportions. A baseline dosage of 5% cementitious material was used in CSM mix proportions. A composite cementitious material, comprising a 6 : 4 mass ratio of GSGS to

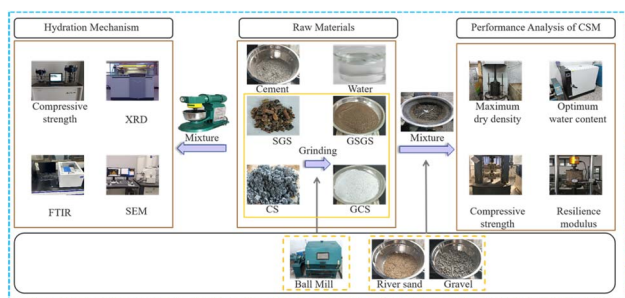


Fig. 1 The test process and main devices.

Table 1 Chemical composition of raw materials (%)

Materials	SiO ₂	Al ₂ O ₃	Fe ₂ O ₃	CaO	MgO	TiO ₂	Na ₂ O	K ₂ O	P ₂ O ₅	SO ₃	LOI
GSGS	47.27	15.23	4.66	7.31	3.65	0.56	1.48	2.14	11.67	—	5.86
GCS	3.23	1.08	0.24	67.9	0.12	0.32	0.13	1.1	—	—	25.88
Cement	16.44	4.79	3.52	61.74	2.87	—	0.20	—	—	3.69	6.75



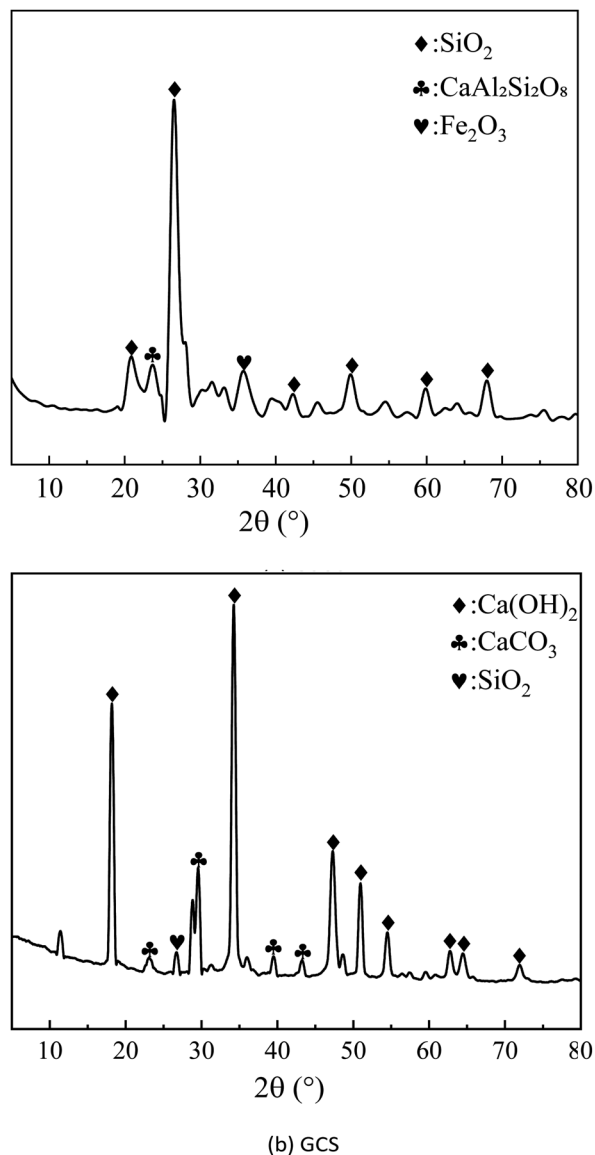


Fig. 2 XRD patterns of raw materials.

GCS, was progressively used to replace cement. Dosage increments of 20% were applied to evaluate the effect of varying cement content on the performance of PSC-CSM. A control group with a pure cement content was included in the comparison. The experimental mix proportions are listed in Table 5.

2.3.2 Mechanical properties. The sample preparation followed the experimental reference specifications for PSC-CSM

(JTG 3441-2024).¹⁹ Cylindrical samples with dimensions of 100 mm × 100 mm (diameter × height) were prepared and stored in plastic bags in a curing room curing at 20 ± 2 °C and 95% relative humidity for 7 and 28 d. Unconfined compressive strength and resilience modulus tests were conducted according to specified experimental procedures.

3 Results and discussion

To better evaluate the effective hydration reaction of sludge gasification slag and carbide slag with cement, the macro (mechanical strength) and micro (XRD, FTIR, SEM-EDS) were tested and analyzed to provide a scientific basis for the hydration mechanism of composite cementitious and then laid the foundation for its application in cement-stabilized macadam. The performance of it (unconfined compressive strength, resilient modulus) is evaluated.

3.1 Mechanical strength of composite cementitious materials

The compressive strength of the composite cementitious materials was investigated at 3 d and 28 d. Fig. 3 illustrates the compressive strength of different samples with varying ratios of GSGS and GCS.

Compressive strength analysis of the samples with varying GSGS-to-GCS ratios revealed notable differences. The 3 d strength of the P30-S10C0 sample was merely 0.7 MPa. After 28 d of curing, its strength increases significantly to 13.7 MPa, indicating that GSGS possesses pozzolanic activity. However excessive content results in low early strength. After 28 d, the later-stage strength of the P30-S10C0 samples showed improvement, suggesting that ground sludge gasification slag reacted with cement to enhance the later-stage strength. Conversely, the P30-S0C10 sample achieves a 3 d strength of 4.7 MPa, but the strength gains diminish over time. Notably, the mixed samples exhibited superior strength at all curing ages compared to the single samples. When the GSGS-to-GCS mass ratio was 6:4, the 28 d strength reached 24.6 MPa, approximately 36% of the strength of the cement paste. This demonstrates a synergistic effect and highlights the effectiveness of the composite modification.

The phenomenon is primarily attributed to the low pozzolanic activity of ground sludge gasification slag in the P30-S10C0 sample, which failed to counteract the dilution effect during the early stages,²⁰ resulting in the low early strength. However, the pozzolanic reaction between it and $\text{Ca}(\text{OH})_2$ effectively activates C-(A)-S-H gel, which markedly enhances the compressive

Table 2 Physical properties of cement

	Apparent density (kg m^{-3})	Specific surface area ($\text{m}^2 \text{kg}^{-1}$)	LOI (%)	Setting time (min)		Compressive strength (MPa)		Flexural strength (MPa)	
				Initial	Final	3 d	28 d	3 d	28 d
Standard value	2800–3100	≥ 300	≤ 5.0	≥ 45	≤ 600	≥ 17	≥ 42.5	≥ 3.5	≥ 6.5
Measured value	3050	343	2.58	184	262	25.7	47.5	5.7	12.3



Table 3 Physical properties of aggregates

Aggregate	Size (mm)	Apparent density (kg m ⁻³)	Bulk density (kg m ⁻³)	Moisture content (%)
Sand	0–5	2583	1512	0.04
Gravel	5–10	2713	1521	0.14

Table 4 Mix proportions of composite cementitious materials

Sample	GSGS : GCS	GSGS (%)	GCS (%)	P (%)
P100	—	—	—	100
P30-S10C0	10 : 0	70	—	30
P30-S0C10	0 : 10	—	70	30
P30-S4C6	4 : 6	28	42	30
P30-S5C5	5 : 5	35	35	30
P30-S6C4	6 : 4	42	28	30
P20-S4C6	4 : 6	32	48	20
P20-S5C5	5 : 5	40	40	20
P20-S6C4	6 : 4	48	32	20
P40-S4C6	4 : 6	24	36	40
P40-S5C5	5 : 5	30	30	40
P40-S6C4	6 : 4	36	24	40

strength at later stages.²¹ In the P30-S0C10 sample, CS increased the alkaline content, markedly promoting early hydration. However, the substantial consumption of CH to form hydration products inhibits further hydration reactions, negatively affecting strength development.²² In contrast, the combination of the two demonstrated superior strength at both the early and late stages compared to the samples with only one component. This synergy arises from the complementary interaction of the materials, which facilitates the rapid and continuous formation of hydration products. These products contribute to a dense and compact microstructure, reduce porosity, and significantly improve strength.²² Further analysis revealed that the samples with a GSGS-to-GCS mass ratio of 6 : 4 exhibited greater late-stage strength than those with a ratio of 5 : 5. This enhancement is attributed to the higher SiO₂ and Al₂O₃ content in there, which increases the Si/Al ratio and improves the efficiency of the synergistic reaction with cement. Additionally, under alkaline conditions, GSGS generates C-(A)-S-H gels and Aft phases, while the dissolution and hydration of silica-alumina phases further enhance the compressive strength.²³

The results of the strength tests on samples with varying ratios indicate the compressive strengths for cement dosages of 20%, 30%, and 40% at 3 and 28 d. The test results are shown in Fig. 4.

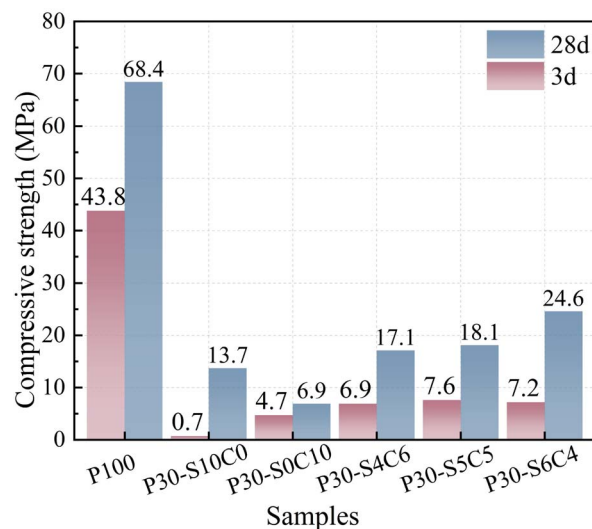


Fig. 3 The compressive strength of samples with different GSGS and GCS ratios.

Fig. 4 illustrates the effect of cement dosage on the compressive strength of the composites. Increasing the cement dosage enhanced the strength in the early and late stages. For a GSGS-to-GCS mass ratio of 4 : 6, samples with 20% cement exhibited strength reductions of 91.55% and 81.43% at 3 and 28 d, respectively, compared to cement paste. With 30% and 40% cement, the reductions decreased to 84.25%, 75%, 69.86%, and 58.92%, respectively. For a mass ratio of 5 : 5, 20% cement reduced the strength by 91.10% and 79.68% at 3 and 28 d, respectively, while 30% and 40% cement reduced the strength to 82.65%, 73.54%, and 74.66% and 55.56%, respectively. At a 6 : 4 mass ratio, 20% cement reduced the strength by 91.78% and 75.58% at 3 and 28 d, respectively, while increasing the cement to 30% and 40% reduced the strength to 83.56%, 64.04%, and 71.92% and 53.22%, respectively. This is likely due to the slower hydration of CaO, SiO₂, and Al₂O₃ at high dosages, limiting the formation of hydration products and strength development.²⁴ Higher cement dosages dilute GSGS and GCS,

Table 5 Mix proportions of the PSC-CSM

Sample	Gravel (g)	Sand (g)	Cement (%)	GSGS-GCS (%)	GSGS : GCS
P100-(SC)0	1950	1050	100	0	—
P80-(SC)20	1950	1050	80	20	6 : 4
P60-(SC)40	1950	1050	60	40	6 : 4
P40-(SC)60	1950	1050	40	60	6 : 4



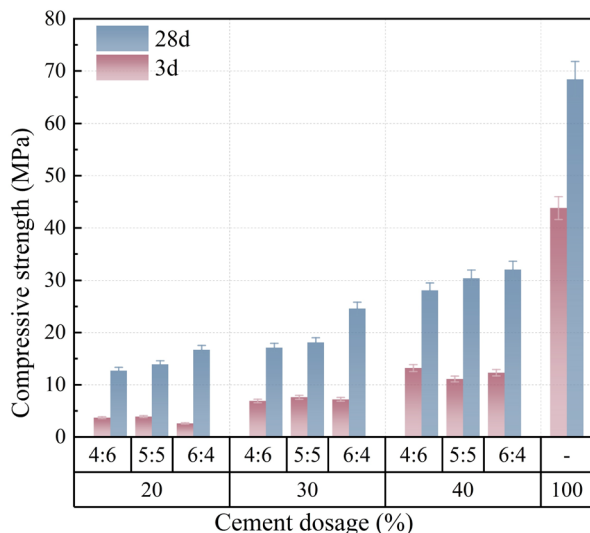


Fig. 4 The compressive strength of samples with different cement dosages.

accelerating hydration and increasing the production of hydration products, thereby improving strength. These results align with those previous studies, which demonstrated delayed strength development at high dosages.

3.2 Microstructure and hydration products analysis

3.2.1 XRD analysis. XRD was conducted to examine the mineral phase changes during the hydration of various samples. The analysis included cement paste, single samples, and mixed samples. The results are shown in Fig. 5.

The XRD results revealed distinct differences in the hydration products of the samples. Compared to the cement paste, the P30-S0C10 sample exhibited significantly higher diffraction peak intensities for $\text{Ca}(\text{OH})_2$. Conversely, the P30-S10C0 sample showed more pronounced SiO_2 diffraction peaks, consistent with the mineral compositions of the raw materials. In the P30-S6C4 sample, the diffraction peak intensities of $\text{Ca}(\text{OH})_2$ and SiO_2 were notably reduced. Despite the 40% GCS dosages, the $\text{Ca}(\text{OH})_2$ diffraction peak intensity in the hydration products of the mixed sample was comparable to that of the cement paste. This indicates that the $\text{Ca}(\text{OH})_2$ from the GCS was consumed by the GSGS and converted into strength-bearing phases, corroborating the strength test results.

High-temperature treatment imparts a low structural order to the silica-aluminum components of GSGS. When mixed with GCS, the alkaline substances promote the dissociation of the silica-aluminum phase, forming $[\text{SiO}_4]^{4-}$ or AlO_2^- ions. This process produces a substantial amount of gel-type hydration products and ettringite (AFt).²⁶ As the curing age increases, the silica-aluminum phases continuously dissolve and hydrate. SiO_2 and Al_2O_3 undergo pozzolanic reactions with the abundant calcium and $\text{Ca}(\text{OH})_2$ in the cement hydration products. These reactions yield rich gels and ettringite, which significantly contribute to compressive strength development at later stages.²⁵ In the P30-S6C4 sample, a synergistic interaction

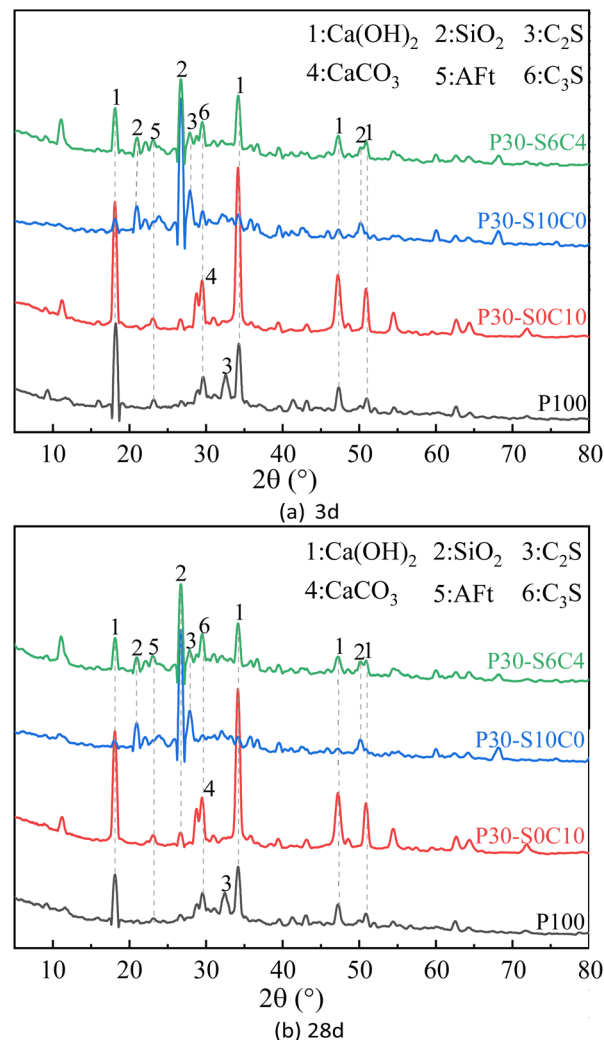


Fig. 5 XRD patterns of samples with different GSGS and GCS ratios. (a) 3 d (b) 28 d.

among the cement, GSGS, and GCS promotes hydration products that fill matrix pores, enhancing the microstructure and macroscopic performance.²⁶

3.2.2 FTIR analysis. FTIR analysis was performed on the four samples to investigate changes in chemical bonds within their hydration products. The results are presented in Fig. 6.

FTIR results show that all composite cementitious materials have a strong absorption peak at 3440 cm^{-1} , attributed to the H-O stretching and bending vibrations in water molecules. The cement paste, P30-S0C10, and P30-S6C4 samples also displayed a peak at 3640 cm^{-1} corresponding to -OH stretching in $\text{Ca}(\text{OH})_2$. The higher intensity of this peak in the P30-S0C10 sample suggests that higher GCS dosages released more OH^- ions. In contrast, the cement paste and P30-S6C4 sample showed reduced -OH content owing to the hydration reactions.²⁷ The absorption peaks at 457 cm^{-1} , 463 cm^{-1} , 534 cm^{-1} , and 570 cm^{-1} in the P30-S10C0 and P30-S6C4 samples are attributed to Si-O-Si symmetric stretching in quartz. The peaks near 1420 cm^{-1} and 875 cm^{-1} in the cement paste, P30-S0C10, and

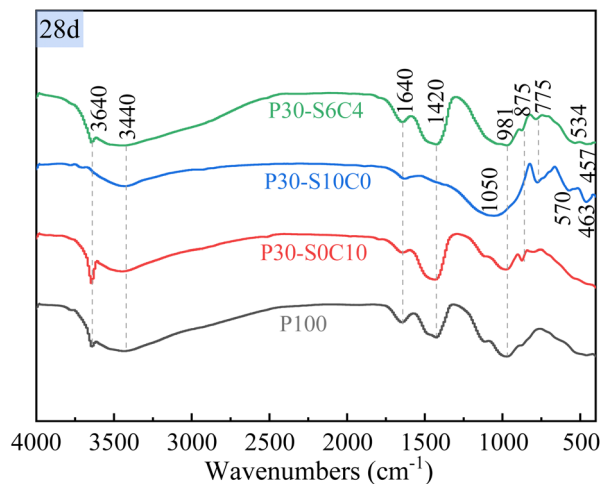


Fig. 6 FTIR pattern of samples with different GSGS and GCS ratios.

P30-S6C4 samples correspond to O–C–O vibrations in CO_3^{2-} , indicating carbonation during sample preparation and curing.²⁸

Further analysis revealed that the absorption peak at 1640 cm^{-1} in all composite cementitious materials and the peak at 1050 cm^{-1} in the P30-S10C0 sample corresponded to O–H vibrations in Aft, indicative of O–H bending and stretching.²⁸ Sharper peaks indicated increased hydration product formation.²⁹ The 981 cm^{-1} peak in the cement paste, P30-S0C10, and P30-S6C4 samples reflects the O–Si–O bending mode in the SiO_4 tetrahedra of C–(A)–S–H gels,²⁸ showing that Aft significantly contributes to the strength of the P30-S10C0 sample. More pronounced peaks for Aft and C–(A)–S–H gels in the cement paste, P30-S0C10 and P30-S6C4 samples suggest enhanced $[\text{SiO}_4]$ stability and polymerization, improving structural integrity.²⁹ The 775 cm^{-1} peak in the P30-S10C0 and P30-S6C4 samples corresponds to Al–O shrinkage vibrations in the AlO_4 tetrahedra, providing key insights into the microstructure of composite cementitious materials.

3.2.3 SEM-EDS analysis. SEM was used to analyze the influence of different mass ratios on the microscopic morphologies of the samples. The results are displayed in Fig. 7.

Fig. 7 reveals that the cement composite materials contain various hydration products, including hexagonal plates, needle bars, grid, fibrous, and flocculent gels.³⁰ Through EDX analysis, the concentrated distribution of Ca and O elements at point 1 in the cement paste (Fig. 7b), combined with its plate morphology, confirms the presence of $\text{Ca}(\text{OH})_2$.³¹ In the P30-S10C0 sample (c and d), the elemental distribution at point 2 (Fig. 7d) shows Ca, Al, S, and O with proportions of 23.2%, 4.2%, 1.5%, and 55%, respectively, which aligns with the elemental composition of Aft.³² This indicates that $\text{Ca}(\text{OH})_2$ formed in the early stages of hydration reacts with SiO_2 to produce a network of fibrous Aft. However, the microstructure is loose, with cracks and unreacted GSGS particles. This is attributed to the low pozzolanic activity of GSGS, leading to incomplete hydration, interrupted reaction continuity, increased internal defects, and reduced later-stage strength.²⁰

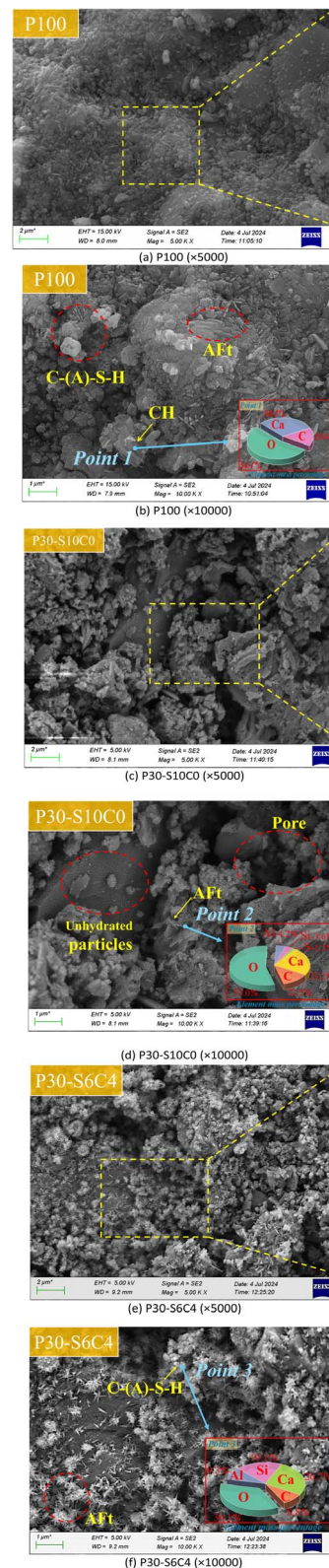


Fig. 7 SEM pattern of samples with different GSGS and GCS ratios. (a) P100 (2 μm) (b) P100 (1 μm) (c) P30-S10C0 (2 μm) (d) P30-S10C0 (1 μm) (e) P30-S6C4 (2 μm) (f) P30-S6C4 (1 μm).

In contrast, the P30-S6C4 sample (e and f) exhibits abundant flocculent gels and needle Aft, interwoven to form a dense, low-porosity structure.³³ At point 3 (Fig. 7f), the proportions of O, Ca,



Si, and Al elements are 36.1%, 26.7%, 19.1%, and 9.3%, respectively, indicating the formation of Al^{3+} containing C-(A)-S-H gel.³⁴ It stems from the interaction between cement and GCS, which collectively creates an alkaline environment, disrupts the network stability of GSGS, accelerates the consumption of $\text{Ca}(\text{OH})_2$, and promotes the formation of Aft and C-(A)-S-H gel.¹⁵ Simultaneously, the Ca^{2+} in GCS significantly enhances the pozzolanic reaction of GSGS, increasing the structural density and mechanical strength.³⁴

3.3 Performance analysis of CSM

3.3.1 Compaction test analysis. Based on the analysis of performance and mechanisms, the optimal replacement cement dosage was identified with a GSGS-to-GCS mass ratio of 6 : 4. The maximum dry density at the optimal water content for this composition is shown in Fig. 8.

The experimental results indicate that the optimum moisture content and maximum dry density of PSC-CSM increase with the addition of GSGS and GCS. This is primarily attributed to the high-water absorption rates of GSGS and GCS, which absorb a portion of the water during the preparation process, thereby enhancing the overall water absorption capacity of the material.³⁵ Furthermore, after deep grinding, the particle size distribution is concentrated in the small particle size range, and their specific surface area is significantly higher than cement. This high specific surface area characteristic enables them to effectively fill the voids in the material, improving overall compactness. These findings are consistent with Ho.³⁶ Therefore, the increased incorporation of GSGS and GCS further optimizes the optimum moisture content and maximum dry density of PSC-CSM.³⁷

Fig. 9 demonstrates that, under the same curing conditions, the performance of PSC-CSM gradually decreases with the increase of GSGS and GCS. However, all samples met the Chinese standard JTG/T F20-2015 requirements. At 0% and 20% dosage, the PSC-CSM satisfies the 7 d unconfined compressive strength (USC) requirement (3.0–5.0 MPa) for heavy traffic loads on highways and grade I bases. When the increase rate is from 0% to 20%, the 7 d UCS decreases by only 0.63% and the elastic modulus decreases by 18.84%, indicating that low increase

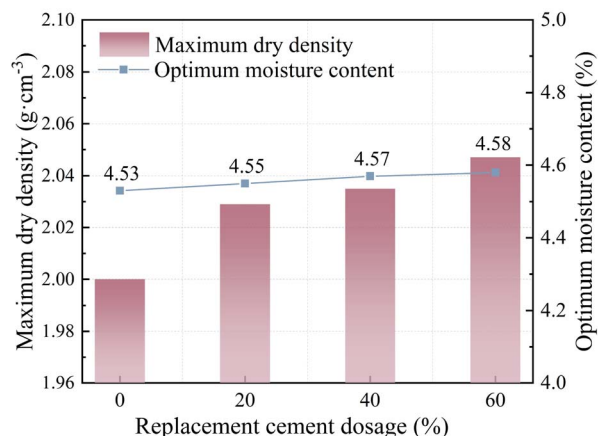


Fig. 8 Influence of GSGS and GCS dosage on the optimum water content and maximum dry density of PSC-CSM.

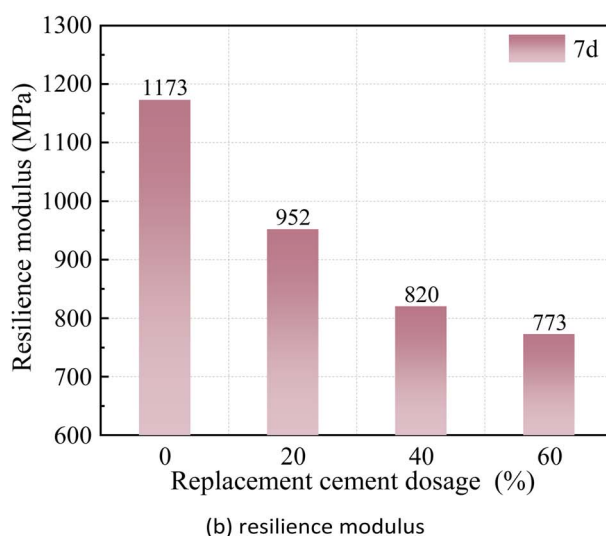
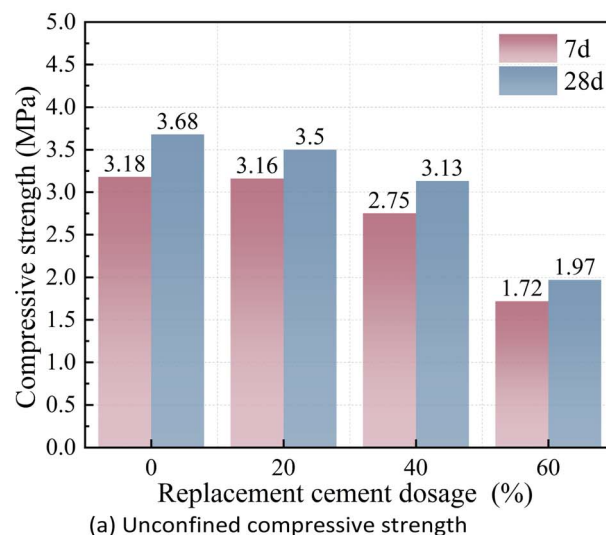


Fig. 9 Influence of GSGS and GCS dosage on the Performance of PSC-CSM. (a) Unconfined compressive strength (b) resilience modulus.

rates have a minor impact on strength but a noticeable reduction in stiffness. Additionally, according to research related to cement production,³⁸ the current price of Portland cement with a 28 d strength of 42.5 MPa is 280 yuan per ton, and the carbon emissions for producing 1 ton of ordinary Portland cement are approximately 735 kg CO_2e . With 20% GSGS-GCS, the cost of cement is reduced by 19% and the carbon emission is reduced by about 20%. Therefore, utilizing sludge gasification slag and carbide slag to prepare cement-stabilized macadam significantly reduces carbon emissions and energy consumption, and reliance on natural resources, meanwhile, demonstrating excellent environmental safety.³⁹

4 Conclusion

This study optimized the composite ratio of GSGS to GCS, revealing their volcanic ash activity and synergistic effect

mechanism in cement-based materials. The results showed that when the mass ratio of GSGS to GCS was 6:4, the 28 d compressive strength of the composite system reached 24.6 MPa, an increase of 53.19% compared to the GSGS alone, equivalent to 36% of the pure cement. At a 20% substitution rate, the mechanical properties of PSC-CSM remain good, with unconfined compressive strength and rebound modulus reduced by only 4% and 18.8%, respectively, while achieving 19% cost savings and 20% carbon reduction. The research results provide a theoretical basis for the resource utilization of SGS and CS, significantly reducing cement consumption and improving resource utilization efficiency. Based on that, this study proposes a technological path for the large-scale application of solid waste in infrastructure construction. Subsequent research will focus on examining the long-term durability (dry shrinkage, freeze–thaw cycles, *etc.*) and engineering applicability of the system, as well as exploring the synergistic effects of multi-component solid waste (fly ash, steel slag, *etc.*) with the GSGS-CS system, to further improve the performance and expand the application field.

Data availability

Data will be made available on request.

Author contributions

Xiaoqi Wang: writing—original draft, data curation, formal analysis; Juntao Ma: methodology, data curation, writing—review and editing; Zhiyong Li: data curation; Kele Wang: data curation; Juntao Ma: methodology, data curation, writing—review and editing; Shunbo Zhao: writing—review and editing; all authors have read and agreed to the published version of the manuscript.

Conflicts of interest

There are no conflicts to declare.

Acknowledgements

This study was funded by the National Natural Science Foundation of China (51508191), the Science and Technology Project of Henan Province (242102321058, 242102321175), Key Scientific Research Project of Henan University (24A560027) and the Colleges Young Teacher Training Project of Henan Province (2023GGJS074).

Notes and references

- 1 S. He, X. J. Huang, P. Yu, Y. T. Zhou and Y. J. Luo, Mechanical properties and durability of alkali-activated fly ash-municipal sludge concrete, *Constr. Build. Mater.*, 2024, **419**, 135515, DOI: [10.1016/j.conbuildmat.2024.135515](https://doi.org/10.1016/j.conbuildmat.2024.135515).
- 2 N. A. Z. Azizan, H. Kamyab, A. Yuzir, N. Abdullah, I. Kirpichnikova, B. Oryani and S. Rezanian, The effects of caffeine, gliclazide, and prazosin on the performance and microbial diversity in an up-flow anaerobic sludge blanket (UASB) reactor, *Biomass Bioenergy*, 2022, **163**, 106511, DOI: [10.1016/j.biombioe.2022.106511](https://doi.org/10.1016/j.biombioe.2022.106511).
- 3 T. Arumugham, A. Yuniarto, N. Abdullah, A. Yuzir, T. M. Aminabhavi, H. Kamyab and Y. Vasseghian, Effective removal of organic substances and nutrients using microgranular sludge in a sequential batch reactor, *J. Water Process Eng.*, 2024, **59**, 105080, DOI: [10.1016/j.jwpe.2024.105080](https://doi.org/10.1016/j.jwpe.2024.105080).
- 4 K. Tanavarotai, H. Kamyab, A. Nor Anuar, T. Khademi, A. Yuzir, V. Ashokkumar and S. Rezanian, Storage and reactivation of aerobic granular sludge: a review, *Fuel*, 2022, **330**, 125536, DOI: [10.1016/j.fuel.2022.125536](https://doi.org/10.1016/j.fuel.2022.125536).
- 5 P. Stolarek and S. Ledakowicz, Thermal processing of sewage sludge by drying, pyrolysis, gasification and combustion, *Water Sci. Technol.*, 2001, **44**, 333–339, DOI: [10.2166/wst.2001.0655](https://doi.org/10.2166/wst.2001.0655).
- 6 L. M. Quan, H. Kamyab, A. Yuzir, V. Ashokkumar, S. E. Hosseini, B. Balasubramanian and I. Kirpichnikova, Review of the application of gasification and combustion technology and waste-to-energy technologies in sewage sludge treatment, *Fuel*, 2022, **316**, 123199, DOI: [10.1016/j.fuel.2022.123199](https://doi.org/10.1016/j.fuel.2022.123199).
- 7 C. Y. Li, X. Y. Zhang, B. X. Zhang, Y. F. Tan and F. L. Li, Reuse of sintered sludge from municipal sewage treatment plants for the production of lightweight aggregate building mortar, *Crystals*, 2021, **11**, 999, DOI: [10.3390/cryst11080999](https://doi.org/10.3390/cryst11080999).
- 8 J. T. Ma, Y. F. Tan and H. Fu, Preparation and Performance of Sludge Gasification Slag Backfill Concrete, *J. Build. Mater. Sci.*, 2024, **27**, 520–527, DOI: [10.3969/j.issn.1007-9629.2024.06.006](https://doi.org/10.3969/j.issn.1007-9629.2024.06.006).
- 9 C. Liang, X. Le, W. Fang, J. Zhao, L. Fang and S. Hou, The Utilization of Recycled Sewage Sludge Ash as a Supplementary Cementitious Material in Mortar: A Review, *Sustainability*, 2022, **14**, 4432, DOI: [10.3390/su14084432](https://doi.org/10.3390/su14084432).
- 10 M. Cyr, M. Coutand and P. Clastres, Technological and environmental behavior of sewage sludge ash (SSA) in cement-based materials, *Cem. Concr. Res.*, 2007, **37**, 1278–1289, DOI: [10.1016/j.cemconres.2007.04.003](https://doi.org/10.1016/j.cemconres.2007.04.003).
- 11 M. Abubakar, Optimization of Cement-Based Mortar Containing Oily Sludge Ash by Response Surface Methodology, *Materials*, 2021, **14**, 6308, DOI: [10.3390/ma14216308](https://doi.org/10.3390/ma14216308).
- 12 K. Z. Fang, D. M. Wang and Y. Gu, Utilization of Gasification Coarse Slag Powder as Cement Partial Replacement: Hydration Kinetics Characteristics, Microstructure and Hardening Properties, *Materials*, 2023, **16**, 1922, DOI: [10.3390/ma16051922](https://doi.org/10.3390/ma16051922).
- 13 Y. X. Guo, W. Y. Hu, G. R. Feng, Y. G. Zhao, C. Q. Li, X. X. Wang and J. H. Ma, Study on the excitation effect and mechanism of coal gasification slag based on solid waste, *Powder Technol.*, 2024, **435**, 119460, DOI: [10.1016/j.powtec.2024.119460](https://doi.org/10.1016/j.powtec.2024.119460).
- 14 H. Li, P. Yan, J. Tian, H. Sun and J. Yin, Study on Mechanical and Frost Resistance Properties of Slag and Macadam



- Stabilized with Cement and Fly Ash, *Materials*, 2021, **14**, 7241, DOI: [10.3390/ma14237241](https://doi.org/10.3390/ma14237241).
- 15 D. Y. Wiranata, S. H. Yang, C. M. Akgul, H. Y. Hsien and M. Z. P. Nugraha, Use of coal ash cement stabilized material as pavement base material: laboratory characterization and field evaluation, *Constr. Build. Mater.*, 2022, **344**, 128055, DOI: [10.1016/j.conbuildmat.2022.128055](https://doi.org/10.1016/j.conbuildmat.2022.128055).
 - 16 Y. P. Liao, Y. Lv, G. Huang, S. L. Ren, X. Y. Wang, R. X. Guo, Y. J. Tian, S. H. Deng and R. S. Lin, Strength and microstructure analysis of subgrade materials containing red sandstone-limestone-cement composites and red sandstone gravel, *Constr. Build. Mater.*, 2024, **416**, 135190, DOI: [10.1016/j.conbuildmat.2024.135190](https://doi.org/10.1016/j.conbuildmat.2024.135190).
 - 17 K. Wang, J. X. Fu and J. Wang, The ratio optimization and hydration mechanism of multi source solid waste cementitious materials, *Constr. Build. Mater.*, 2024, **411**, 134267, DOI: [10.1016/j.conbuildmat.2023.134267](https://doi.org/10.1016/j.conbuildmat.2023.134267).
 - 18 J. Yue, X. Nie, Z. Wang, J. Liu and Y. Huang, Research on the Pavement Performance of Slag/Fly Ash-Based Geopolymer-Stabilized Macadam, *Appl. Sci.*, 2022, **12**, 10000, DOI: [10.3390/app121910000](https://doi.org/10.3390/app121910000).
 - 19 JTG 3441-2024, *Test Code for Inorganic Binder Stabilized Materials in Highway engineering[S]*, Ministry of Transport of the People's Republic of China, Beijing, 2024.
 - 20 B. F. Zhang, F. Muhammad, T. Yu, M. Fahimzadeh, M. A. S. Hassan, J. K. Liang, X. A. Ning and P. Yuan, Harnessing iron tailings as supplementary cementitious materials in Limestone Calcined Clay Cement (LC3): An innovative approach towards sustainable construction, *Constr. Build. Mater.*, 2024, **453**, 139111, DOI: [10.1016/j.conbuildmat.2024.139111](https://doi.org/10.1016/j.conbuildmat.2024.139111).
 - 21 Yu Liu, Z. G. Yan, C. W. K. Chow, A. Keegan, P. N. Pham, D. D. Li, J. A. Oh, R. Siddique and S. Rafat, The potential use of drinking water sludge ash as supplementary cementitious material in the manufacture of concrete blocks, *Resour. Conserv.*, 2020, **168**, 105291, DOI: [10.1016/j.RESCONREC.2020.105291](https://doi.org/10.1016/j.RESCONREC.2020.105291).
 - 22 J. Q. Zhang, Q. Luo and X. Y. Zhang, Exploring the influence of calcined clay grade on the rheological dynamics of LC3 mortar, *Constr. Build. Mater.*, 2024, **444**, 137852, DOI: [10.1016/j.conbuildmat.2024.137852](https://doi.org/10.1016/j.conbuildmat.2024.137852).
 - 23 W. Zhang, X. S. Hao, C. Wei, X. M. Liu and Z. Q. Zhang, Activation of low-activity calcium silicate in converter steelmaking slag based on synergy of multiple solid wastes in cementitious material, *Constr. Build. Mater.*, 2022, **351**, 128925, DOI: [10.1016/j.conbuildmat.2022.128925](https://doi.org/10.1016/j.conbuildmat.2022.128925).
 - 24 Y. Y. Bai, W. C. Guo, Q. X. Zhao, H. Y. Shen and Y. X. Qiu, Strength formation mechanism and curing system optimization of low-carbon cementitious materials prepared by synergistic activation of multiple alkaline solid wastes, *Constr. Build. Mater.*, 2023, **402**, 132931, DOI: [10.1016/j.conbuildmat.2023.132931](https://doi.org/10.1016/j.conbuildmat.2023.132931).
 - 25 J. H. Zhao, Z. H. Li, D. M. Wang, P. Y. Yan, L. Luo, H. W. Zhang, H. M. Zhang and X. B. Gu, Hydration superposition effect and mechanism of steel slag powder and granulated blast furnace slag powder, *Constr. Build. Mater.*, 2023, **366**, 130101, DOI: [10.1016/j.conbuildmat.2022.130101](https://doi.org/10.1016/j.conbuildmat.2022.130101).
 - 26 H. S. Jiang, G. J. Ke and Z. Y. Li, Synergistic activation mechanism and long-term properties of a solid waste cementitious materials based on red mud and calcium carbide slag, *Constr. Build. Mater.*, 2024, **438**, 137313, DOI: [10.1016/j.conbuildmat.2024.137313](https://doi.org/10.1016/j.conbuildmat.2024.137313).
 - 27 Y. X. Shi, Q. X. Zhao, C. H. Xue, Y. L. Jia, W. C. Guo, Y. Y. Zhang and Y. X. Qiu, Preparation and curing method of red mud-calcium carbide slag synergistically activated fly ash-ground granulated blast furnace slag based eco-friendly geopolymer, *Constr. Build. Mater.*, 2023, **139**, 104999, DOI: [10.1016/j.cemconcomp.2023.104999](https://doi.org/10.1016/j.cemconcomp.2023.104999).
 - 28 M. Wu, Y. S. Zhang, Y. T. Jia, W. She, G. J. Liu, Z. Q. Yang, Y. Zhang, W. T. Zhang and W. Sun, Effects of sodium sulfate on the hydration and properties of lime-based low carbon cementitious materials, *J. Cleaner Prod.*, 2019, **220**, 677–687, DOI: [10.1016/j.jclepro.2019.02.186](https://doi.org/10.1016/j.jclepro.2019.02.186).
 - 29 X. Y. Wang, X. Y. Wang, J. Z. Lv, J. C. Yang, B. He, P. J. Han and X. H. Bai, Mechanical properties and hydration behaviour of circulating fluidised bed fly ash-ground granulated blast furnace slag-lime ecofriendly cementitious material, *Constr. Build. Mater.*, 2023, **409**, 133964, DOI: [10.1016/j.conbuildmat.2023.133964](https://doi.org/10.1016/j.conbuildmat.2023.133964).
 - 30 S. H. Cui, K. J. Fan and Y. Yao, Preparation and characterization of quaternary clinker-free cementitious materials containing phosphorus slag, calcium carbide slag, desulfurization gypsum, and metakaolin, *Constr. Build. Mater.*, 2024, **411**, 134602, DOI: [10.1016/j.conbuildmat.2023.134602](https://doi.org/10.1016/j.conbuildmat.2023.134602).
 - 31 K. L. Scrivener and A. Nonat, Hydration of cementitious materials, present and future, *Cem. Concr. Res.*, 2011, **41**, 651–665, DOI: [10.1016/j.cemconres.2011.03.026](https://doi.org/10.1016/j.cemconres.2011.03.026).
 - 32 B. Lothenbach, K. Scrivener and R. D. Hooton, Supplementary cementitious materials, *Cem. Concr. Res.*, 2011, **41**, 1244–1256, DOI: [10.1016/j.cemconres.2010.12.001](https://doi.org/10.1016/j.cemconres.2010.12.001).
 - 33 Y. Deng, X. Wang, B. Zhou, X. Xu and L. Chen, Systematic assessment of a multi-solid waste cementitious material: feasibility and environmental impact, *Constr. Build. Mater.*, 2024, **428**, 136323, DOI: [10.1016/j.conbuildmat.2024.136323](https://doi.org/10.1016/j.conbuildmat.2024.136323).
 - 34 C. C. Dharmawardhana, A. Misra and W. Ching, Theoretical investigation of C-(A)-SH (I) cement hydrates, *Constr. Build. Mater.*, 2018, **184**, 536–548, DOI: [10.1016/j.conbuildmat.2018.07.004](https://doi.org/10.1016/j.conbuildmat.2018.07.004).
 - 35 P. F. Yan, Z. G. Ma, H. B. Li, P. Gong, M. Xu and T. Chen, Laboratory tests, field application and carbon footprint assessment of cement-stabilized pure coal solid wastes as pavement base materials, *Constr. Build. Mater.*, 2023, **366**, 130265, DOI: [10.1016/j.conbuildmat.2022.130265](https://doi.org/10.1016/j.conbuildmat.2022.130265).
 - 36 M. Hoy, D. V. Nhieu, S. Horpibulsuk, A. Suddeepong, A. Chinkulkijniwat, A. Buritatum and A. Arulrajah, Effect of wetting and drying cycles on mechanical strength of cement-natural rubber latex stabilized recycled concrete aggregate, *Constr. Build. Mater.*, 2023, **394**, 132301, DOI: [10.1016/j.conbuildmat.2023.132301](https://doi.org/10.1016/j.conbuildmat.2023.132301).



- 37 S. H. Zhou, H. K. Luo, B. P. Feng, W. T. Zheng, C. R. Zeng, W. Z. Zhang, J. Liu and F. Xing, Research on using municipal solid waste incineration bottom ash for cement-stabilized macadam, *Constr. Build. Mater.*, 2024, **425**, 135850, DOI: [10.1016/j.conbuildmat.2024.135850](https://doi.org/10.1016/j.conbuildmat.2024.135850).
- 38 J. Wang, Y. Ding, Y. Zhou, W. Wei and Y. Wang, Municipal solid waste incineration bottom ash recycling assessment: Carbon emission analysis of bottom ash applied to pavement materials, *Constr. Build. Mater.*, 2024, **421**, 135774, DOI: [10.1016/j.conbuildmat.2024.135774](https://doi.org/10.1016/j.conbuildmat.2024.135774).
- 39 A. Mohammadi and A. M. Ramezani pour, Investigating the environmental and economic impacts of using supplementary cementitious materials (SCMs) using the life cycle approach, *J. Build. Eng.*, 2023, **79**, 107934, DOI: [10.1016/j.jobbe.2023.107934](https://doi.org/10.1016/j.jobbe.2023.107934).

